ISSN 1995-0780, Nanotechnologies in Russia, 2019, Vol. 14, Nos. 5–6, pp. 190–196. © Pleiades Publishing, Ltd., 2019.
Russian Text © The Author(s), 2019, published in Rossiiskie Nanotekhnologii, 2019, Vol. 14, Nos. 5–6.

FUNCTIONAL AND CONSTRUCTION NANOMATERIALS

High Photocatalytic Activity Nanomaterials Based on Titanium Dioxide

E. A. Konstantinova[a,b,c,*], M. P. Kushnikov[a], V. B. Zaitsev[a], V. G. Kytin[a], A. V. Marikutsa[a], G. V. Trusov[d], A. S. Sedegov[d], and P. K. Kashkarov[a,b,c]

[a] *Moscow State University, Moscow, 119991 Russia*
[b] *National Research Center Kurchatov Institute, Moscow, 123098 Russia*
[c] *Moscow Institute of Physics and Technology, Dolgoprudny, 141701 Russia*
[d] *National University of Science and Technology MISIS, Moscow, 119049 Russia*
**e-mail: liza35@mail.ru*

Received September 20, 2019; revised September 20, 2019; accepted September 20, 2019

Abstract—X-ray diffraction, optical spectroscopy, and electron paramagnetic resonance (EPR) have been used to study microspheres and nanoheterostructures based on titanium dioxide synthesized by aerosol pyrolysis and sol–gel methods. All test samples are characterized by a large specific surface area (about 100 m^2/g of substance). It was established that the main type of radicals in the resulting structures are $N^{\bullet}$, $NO^{\bullet}$, as well as Ti^{3+}, Mo^{5+}, V^{4+}, and W^{5+} centers. Microspheres and nanoheterostructures consisting of several metal oxides have high photocatalytic activity in the visible spectrum and the ability to accumulate photogenerated charge carriers. As a result, catalytic reactions in the samples continue even after illumination is turned off. A correlation was found between the rate of photocatalysis and the radical concentration in the studied structures. The results can be used to develop new-generation energy-efficient catalytic devices based on nanocrystalline titanium oxide, which operate in the visible range and do not require continuous illumination.

DOI: 10.1134/S1995078019030078

INTRODUCTION

For many years, titanium dioxide (TiO_2) has been the focus of researchers [1–5]. In the 21st century, nanocrystalline TiO_2 obtained by various synthesis methods [2–6] is being actively studied. In the last decade, combined structures containing TiO_2 have generated the most interest among them, it is important to note such systems as the core/shell [3, 7]; nanoheterostructures consisting of two or three metal nanooxides (differing in chemical composition) and representing a set of discrete oxide/oxide nanoheterojunctions, one of which is nanocrystalline titanium dioxide, which has the highest photoactivity among all known metal oxides [8, 9]; and microspheres and ordered ensembles of nanocrystals of various metal oxides (from one to four) [10]. As the latter, molybdenum (MoO_3), vanadium (V_2O_5), and tungsten (WO_3) oxides are used. The constantly growing interest in TiO_2, as well as systems based on it, is primarily due to this material's unusual properties, among which one to be noted is the very developed surface with an area that varies, depending on the synthesis method, from tens to hundreds of square meters per gram of substance, and is open to ambient molecules, as well as photocatalysis ability [5, 11–14]. The latter results from the fact that illumination generates TiO_2 under the influence of illumination of radicals in TiO_2 (when adsorbed water and oxygen molecules interact with photoexcited electrons and holes), which participate in redox reactions, as a result of which organic substances (including toxic ones) in contact with the TiO_2 surface break down into simple constituents—carbon dioxide and water [11–14]. In addition, when these reactions occur, viruses and bacteria are destroyed [3, 8]. This property of TiO_2 is used to create photocatalytic filters for air purification from undesirable impurities [5]. However, these devices have a number of significant disadvantages, among which is the need for a UV lamp as a light source, since TiO_2 is a wide-gap semiconductor (the band gap varies from 3.1 to 3.5 eV), the need for continuous illumination during operation of the photocatalyst, and, ultimately, the high cost of the filter.

Currently, the scientific community is actively working to overcome these shortcomings: TiO_2 doped with atoms of various metals and nonmetals to increase absorption in the visible spectral range [5, 15–19] or TiO_2 combined with other metal oxides [3, 8, 9]. The latter can significantly increase the lifetime of photoexcited charge carriers as a result of their

spatial separation, which prevents recombination. This is achieved as follows. From the most photosensitive TiO_2 (as a part of nanoheterojunctions), photoexcited electrons are injected into another metal oxide; as a result, electron–hole recombination is suppressed. However, there is still no comprehensive approach to synthesizing TiO_2-based nanomaterials that simultaneously combines doping of TiO_2 and combination with various metal oxides also having photocatalytic properties. This study is dedicated to solving this problem. By varying the synthesis parameters, we were able to obtain structures with a high concentration of radicals that effectively absorb in the visible spectrum and are characterized by high photocatalytic reaction rates.

EXPERIMENTAL

The studied samples were formed by two different methods: aerosol pyrolysis and sol–gel.

For the preparation of microspheres consisting of TiO_2, MoO_3, WO_3, V_2O_5, TiO_2/MoO_3, TiO_2/WO_3, TiO_2/V_2O_5, and $TiO_2/MoO_3/V_2O_5$, the relatively new method of aerosol pyrolysis was used, described in detail in [7, 10]. The installation consisted of a gas flow regulator (RRG-10, Eltochpribor, Russia) with a dust filter and a control unit; an ultrasonic atomizer (IN-8, Albedo, Russia) to generate aqueous aerosols of the reaction mixtures; a tube laboratory furnace (SUOL-0.4.4/12-M2-U4.2) with a quartz reactor and a Schott filter with a pore size of 1–10 μm for trapping the pyrolysis products. The operating frequency of the piezoelectric emitter was 2.64 MHz, the aerosol productivity was from 0 to 6 mL/min, and the average value of the mass-median aerodynamic particle diameter (MMAD) of the aerosol was 3.94 μm. The temperature in the furnace was controlled by a built-in thermocouple. The length of the working part of the reactor is 700 mm, the length of the isothermal region is 500 mm, and the inner diameter is 45 mm. As metal precursors, titanyl nitrate, ammonium paratungstate, ammonium paramolybdate, and ammonium metavanadate were used; urea was used as a dopant.

Nitrogen-doped nanocrystalline TiO_2 in the form of an aqueous sol was prepared by controlled hydrolysis by dropwise addition of 12.5% NH_4OH to 2.5 M of an aqueous solution of $TiCl_4$ + 0.65 M HCl cooled to 0°C with vigorous stirring until pH 5. The resulting precipitate was washed with distilled water and dispersed by ultrasonic treatment. The gel precipitate was placed in an oven in a cup, then annealed in an oven at 450°C and triturated. To obtain nanoheterostructures of TiO_2/MoO_3, $TiO_2/MoO_3/WO_3$, and $TiO_2/MoO_3/V_2O_5$, we dissolved $(NH_4)_6Mo_7O_{24}$, $(NH_4)_{10}W_{12}O_{41} \cdot 4.5H_2O$, and NH_4VO_3 in a mixture of hydrochloric acid and hydrogen peroxide; these solutions were mixed with precipitated TiO_2, then dried and annealed at 450°C.

The specific surface area of the samples was measured by nitrogen adsorption: the Brunauer–Emmett–Teller (BET) method using a Chemisorb 2750 instrument (Micromeritics). The diffuse light scattering spectra from the obtained samples were recorded with an LS-55 PerkinElmer spectrograph operating in the spectral range of 200–900 nm with a spectral slit width from 2.5 to 20 nm. X-ray diffraction (XRD) was measured with a DRON-4 diffractometer (CuK_α-radiation). When calculating the CSR using the Scherrer formula, the full width at half maximum was used, and the instrumental spreading was 0.09°.

The EPR spectra were recorded on a Bruker ELEXSYS 500 EPR spectrometer (Germany) (operating frequency 9.5 GHz, X-band, sensitivity 5×10^{10} spin/G). Samples were placed in quartz ampoules with a diameter of 4 mm. To conduct EPR experiments in dark–illumination–dark cycles, an optical resonator was used. Samples were illuminated directly in the spectrometer cavity with a Bruker ELEXSYS ER 202 UV high-pressure mercury lamp (power 50 W). To isolate the visible region, cutoff filters were used. An MDR-3 monochromator was used to irradiate samples with light quanta at a given wavelength. The photoexcitation intensity of the samples was approximately 15 mW/cm^2. The measurements were carried out at a temperature of 77 K. To preliminarily assess the g factors, we used reference MgO containing Mn^{++} ions. To determine the number of spin centers, the EPR signals from the test sample were compared with the spectra of the standard $CuCl_2 \cdot 2H_2O$. Theoretical processing of the EPR spectra was carried out in MatLab with the EasySpin plugin [20].

To determine the photocatalytic activity (oxidizing ability) of the samples, the photodegradation reaction of Rhodamine 6G dye was used. For this, the dye was applied to the surface of the titanium dioxide from an aqueous solution. The change in surface concentration of the dye was monitored by diffuse reflection R at a wavelength of 530 nm (corresponding to maximum absorption of the adsorbed dye). Diffuse reflection was converted to a value proportional to the surface concentration ($\sim(1 - R)^2/2R$), according to the Kubelka–Munk formula [21].

RESULTS AND DISCUSSION

Microspheres of TiO_2, MoO_3, WO_3, and V_2O_5 based on the data obtained using BET had a specific surface area of 55 ± 6, 82 ± 8, 70 ± 7, and 65 ± 7 m^2/g, respectively. Compound microspheres of TiO_2/MoO_3, TiO_2/WO_3, TiO_2/V_2O_5, $TiO_2/MoO_3/V_2O_5$ were characterized by specific surface areas of 75 ± 8, 62 ± 6, 65 ± 7, and 60 ± 6 m^2/g, respectively. For nanoheterostructures, the following specific surface areas were obtained: 110 ± 10 (TiO_2/MoO_3), 100 ± 10

($TiO_2/MoO_3/WO_3$), and 95 ± 10 ($TiO_2/MoO_3/V_2O_5$) m^2/g.

According the XRD data, in the microspheres, titanium dioxide has two phases: anatase and rutile; in nanoheterostructures, only anatase modification is present. The sizes of nanoparticles calculated from line broadening in diffractograms using the Scherrer formula are presented below. For microspheres: 20 ± 2 nm (TiO_2), 15 ± 2 nm (MoO_3), 12 ± 1 nm (WO_3), 13 ± 1 nm (V_2O_5), 12 ± 2/10 ± 2 nm (TiO_2/MoO_3), 10.5 ± 1/5.5 ± 1 nm (TiO_2/WO_3), 11.5 ± 1/7.5 ± 2 nm (TiO_2/V_2O_5), 10 ± 1/7 ± 1/6 ± 1 nm ($TiO_2/MoO_3/V_2O_5$); for nanoheterostructures: 4 ± 0.5 nm (TiO_2/MoO_3), 3.7 ± 0.5 nm ($TiO_2/MoO_3/WO_3$), 9 ± 1 nm ($TiO_2/MoO_3/V_2O_5$). Note that the presence of molybdenum, tungsten, and vanadium oxide phases in nanoheterostructures has not been unambiguously determined by XRD analysis, probably due to the too low intensity of the corresponding peaks.

Let us discuss the experimental results obtained by EPR spectroscopy. Figure 1a shows the EPR spectra of microspheres consisting of the same type of metal oxides: TiO_2, WO_3, MoO_3.

As can be seen from Fig. 1a, the EPR signal of TiO_2 samples (spectrum *1*) has a complex shape. Therefore, to determine the nature of the detected radicals, computer simulation was performed. The following parameters of the EPR lines are given: *g*-tensor, $g_1 = 2.0082$, $g_2 = 2.0039$, $g_3 = 2.0036$; the EPR linewidth is $\Delta H_1 = 1.33$ G, $\Delta H_2 = 0.35$ G, $\Delta H_3 = 2.1$ G; and hyperfine coupling constants (HCC) $A_1 = 1.6$ G, $A_2 = 1.1$ G, $A_3 = 22.5$ G. EPR signals with such parameters in accordance with the data of [22–24] can be attributed to nitrogen atoms $N^\bullet$ (nuclear spin $I = 1$) with uncompensated electron spin, which were introduced into TiO_2 during synthesis. WO_3 samples are characterized by an EPR signal with a low intensity and complex shape. As a result of computer simulation, we obtained the following parameters of the EPR spectrum: $g_1 = 2.0039$, $g_2 = 1.999$, $g_3 = 1.928$, $\Delta H_1 = 18.5$ G, $\Delta H_2 = 9.3$ G, $\Delta H_3 = 22.7$ G, $A_1 = 0.5$ G, $A_2 = 21$ G, $A_3 = 6$ G. According to [22–24], it can be concluded that in WO_3 microspheres the nitrogen monoxide ($NO^\bullet$) radical is detected, which is formed from introduction of nitrogen atoms into the tungsten oxide structure during synthesis. Lastly, the EPR spectrum of the MoO_3 samples is the superposition of several overlapping EPR signals from different radicals. Therefore, we again resorted to a theoretical analysis of this experimental spectrum and obtained the following parameters of the EPR signals (identification of the EPR lines shown in Fig. 1a, the spectrum *3*, shown from left to right, the lines partially overlap): O_2^- radicals $g_1 = 2.025$, $g_2 = 2.010$, $g_3 = 2.003$, $\Delta H_1 = 24$ G, $\Delta H_2 = 21$ G [22, 25]; $N^\bullet$ radicals; $NO^\bullet$ radicals; Ti^{3+}/oxygen vacancy centers $g_1 = 1.9935$, $H_1 = 85$ G, $g_2 = 1.9328$, $H_2 = 112$ G [22]; Mo^{5+} radicals $g_1 = 1.943$, $g_2 = 1.863$, $\Delta H_1 = 39$ G, $\Delta H_2 = 43$ G, $A_1 = 45$ G, $A_2 = 15$ G [22]. The concentration of radicals calculated in this study (N_s) had the following values: 5×10^{16} g^{-1} (TiO_2), 1.3×10^{15} g^{-1} (WO_3), 1.5×10^{17} g^{-1} (MoO_3).

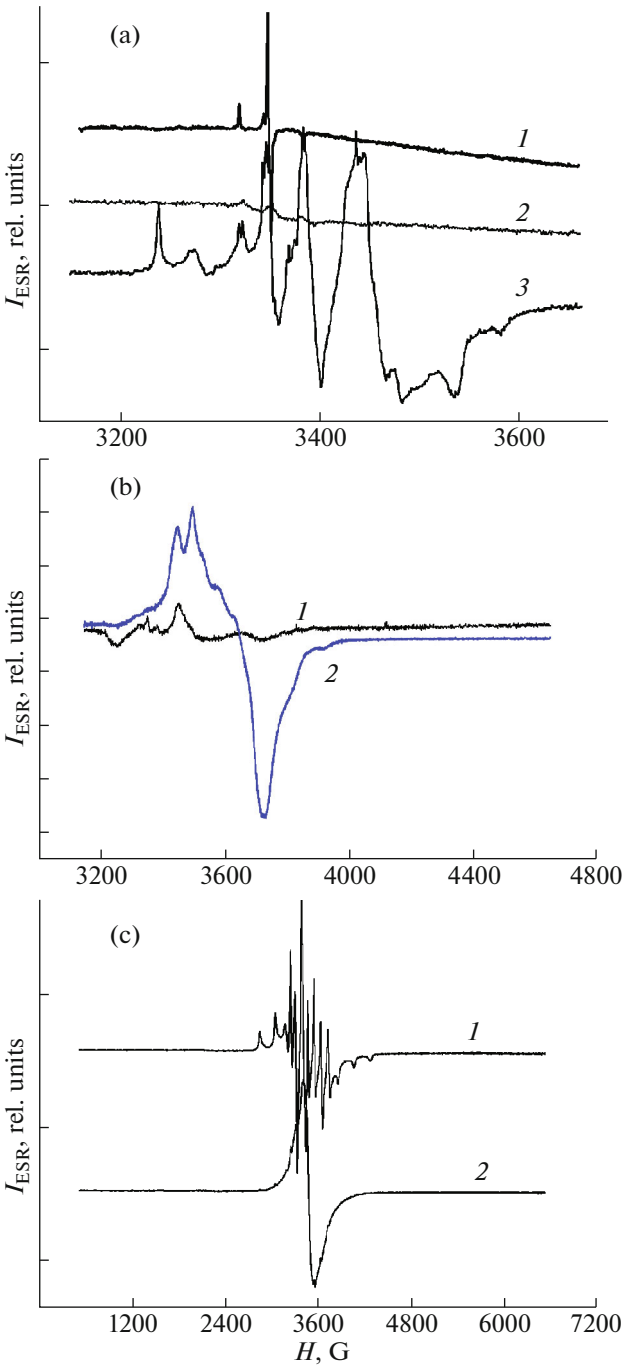

Fig. 1. (Color online) EPR spectra of microspheres: (a) TiO_2 (*1*), WO_3 (*2*), MoO_3 (*3*); (b) TiO_2/WO_3 (*1*), TiO_2/MoO_3 (*2*); (c) TiO_2/V_2O_5 (*1*), $TiO_2/MoO_3/V_2O_5$ (*2*). Recording temperature 77 K.

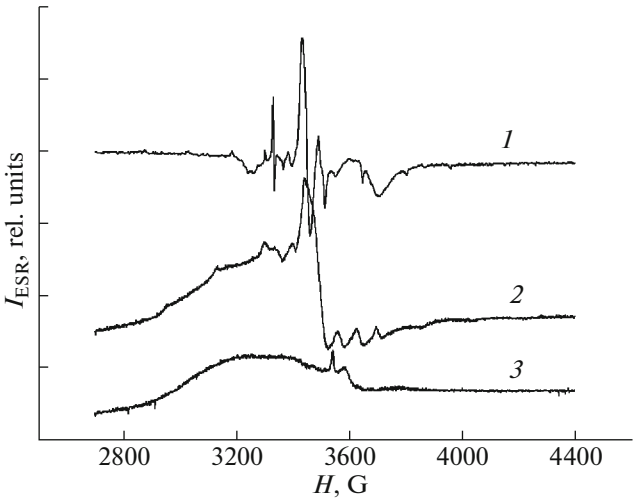

Fig. 2. EPR spectra of TiO_2/MoO_3 (*1*), $TiO_2/MoO_3/V_2O_5$ (*2*), $TiO_2/MoO_3/WO_3$ (*3*) nanoheterostructures. Recording temperature 77 K.

The EPR spectra of TiO_2/WO_3 and TiO_2/MoO_3 microspheres are shown in Fig. 1b.

We first discuss the EPR spectrum of the TiO_2/WO_3 samples, which is a superposition of several overlapping EPR signals with various parameters (interpretation from left to right in Fig. 1b): $N^\bullet$ radicals; $NO^\bullet$ radicals; W^{5+} radicals $g_1 = 1.88$, $g_2 = 1.83$, $g_3 = 1.8$, $\Delta H_1 = 64$ G, $\Delta H_2 = 38$ G, $\Delta H_3 = 88$ G [26]. In TiO_2/MoO_3 microspheres, superposition of the EPR spectrum of significantly higher intensity is also observed in comparison with TiO_2/WO_3 structures. According to the computer simulation data, it is characterized by the following parameters: $N^\bullet$ radicals; $NO^\bullet$ radicals; Ti^{3+}/oxygen vacancy centers; Mo^{5+} radicals; surface Mo^{5+} radicals $g_1 = 1.921$, $g_2 = 1.784$, $\Delta H_1 = 48$ G, $\Delta H_2 = 57$ G, $A_1 = 48$ G, $A_2 = 27$ G [26]. For the samples shown in Fig. 1b, the N_s values were also calculated: 9×10^{16} g^{-1} (TiO_2/WO_3), 8×10^{17} g^{-1} (TiO_2/MoO_3).

The EPR spectra of TiO_2/V_2O_5 and $TiO_2/MoO_3/V_2O_5$ microspheres are shown in Fig. 1c and also have a complex structure. A theoretical analysis of these data showed that the EPR spectrum of the TiO_2/V_2O_5 sample result from the superposition of contributions from $N^\bullet$ and V^{4+} radicals ($g_1 = 1.993$, $g_2 = 1.949$, $\Delta H_1 = 27.5$ G, $\Delta H_2 = 18$ G, $A_1 = 53$ G, $A_2 = 150$ G) [27, 28]. The EPR spectrum of the $TiO_2/MoO_3/V_2O_5$ sample was strongly broadened, probably due to spin-exchange interaction, which usually takes place in systems with a high local concentration of radicals (spin centers) [29]. As a result of computer simulation, the following EPR spectrum parameters were recovered: $N^\bullet$ radicals; Mo^{5+} radicals; V^{4+} radicals. The samples shown in Fig. 1c are characterized by the following concentrations N_s: 7×10^{17} g^{-1} (TiO_2/V_2O_5), 3.8×10^{18} g^{-1} ($TiO_2/MoO_3/V_2O_5$).

The EPR spectra of TiO_2/MoO_3, $TiO_2/MoO_3/V_2O_5$, $TiO_2/MoO_3/WO_3$ nanoheterostructures are shown in Fig. 2 and are the superposition of EPR signals from different radicals.

In the TiO_2/MoO_3 samples, the following radicals were found: $N^\bullet$; Ti^{3+}/oxygen vacancy; Mo^5. $TiO_2/MoO_3/V_2O_5$ heterostructures are characterized by superposed spin centers, such as $N^\bullet$; Ti^{3+}/oxygen vacancy; Mo^{5+}; V^{4+}. The calculated N_s concentrations had the following values: 2×10^{18} g^{-1} (TiO_2/MoO_3), 1.5×10^{19} g^{-1} ($TiO_2/MoO_3/V_2O_5$), 1.3×10^{17} g^{-1} ($TiO_2/MoO_3/WO_3$).

Since the topic of this work is the development and study of energy-efficient nanomaterials based on titanium dioxide with a high degree of photocatalytic activity in the visible region, the photocatalysis kinetics were measured using the studied structures when they were irradiated with light in the wavelength range $\Delta\lambda = 400$–750 nm. The photodegradation reaction of Rhodamine 6G dye was used as the test reaction. The results are shown in Fig. 3. As follows from Fig. 3a, the highest photocatalytic activity among $WO_3/MoO_3/TiO_2$ microspheres were the TiO_2 samples. This may be due to both the high concentration of radicals participating in redox reactions on the surface of the photocatalyst and the lower recombination rate of photoexcited electrons and holes in TiO_2 in comparison with other studied metal oxides [12]. After illumination was turned off ($t = 20$ min), dye degradation ceased.

Analysis of Fig. 3b shows that in the series of TiO_2/WO_3, TiO_2/V_2O_5, TiO_2/MoO_3, $TiO_2/MoO_3/V_2O_5$ microspheres, the first three samples are characterized by approximately the same photocatalysis rates, while triple microspheres have the highest photoactivity in the visible range.

Comparative analysis of the N_s values of this series of samples showed that the $TiO_2/MoO_3/V_2O_5$ structures have the largest N_s values. The revealed tendency of correlation between the photocatalysis rate and the concentration of radicals in the samples also occurs in the series of TiO_2/MoO_3, $TiO_2/MoO_3/V_2O_5$, $TiO_2/MoO_3/WO_3$ (Fig. 3c).

Indeed, the $TiO_2/MoO_3/V_2O_5$ samples have the maximum N_s value in this series. After illumination is turned off ($t = 20$ min), the dye degradation process continued in the microspheres consisting of several metal oxides and nanoheterostructures (Figs. 3b and 3c). This indicates that the recombination of photoexcited electrons and holes was suppressed. It can be assumed that electrons from TiO_2 are injected into WO_3, MoO_3, V_2O_5. As a result, electrons and holes will

be spatially separated, which dramatically reduces the recombination rate. Thus, the obtained samples exhibit catalytic activity even after illumination is turned off, which indicates their energy efficiency.

Note that large concentrations of radicals not only affect the rate of photocatalytic reactions, but can also be responsible for increasing the absorption coefficient of samples in the visible range. The latter, in turn, also leads to an increase in the photocatalysis rate. Therefore, in this work, we studied the coefficient of light absorption by samples of microspheres and nanoheterostructures. We investigated the spectra of diffuse light scattering from all samples in the range from 250 to 700 nm. From these data, using the spectrum of a reference white sample, light absorption spectra were obtained for the studied nanostructures. The band gap values E_g of these structures were determined using Kubelka and Munk's two-component theory [21] (under the assumption that the irradiating light is monochromatic and the diffusely reflected radiation is isotropic). According to this theory, diffuse reflection R of the sample depends only on the ratio of the absorption coefficient α and the scattering coefficient S, and not separately from the scattering coefficient or absorption coefficient:

$$\frac{\alpha}{S} = \frac{(1-R)^2}{2R} = F(R),$$

where $F(R)$ is the Kubelka–Munk function.

To determine the band gap, the experimental data were represented as the dependence

$$(\alpha h\nu)^2 = A^2(h\nu),$$

where A is a constant, h is the Planck constant, and ν is the radiation frequency. Band gap E_g was determined from the intersection point of the linear extrapolation of this dependence with the abscissa axis. As an example, Fig. 4 shows the construction of the function $(\alpha h\nu)^2$ depending on the energy of quanta $h\nu$ and the band gap for microspheres TiO_2 obtained by aerosol pyrolysis.

According to the calculations, the band gap for the indicated TiO_2 microspheres is 3.08 ± 0.03 eV. The band gap determined by a similar method for TiO_2 microspheres doped with nitrogen did not differ much: 3.22 ± 0.03 eV.

The band gap of molybdenum(VI) nanooxide is much wider than that of titanium oxide; its width is about 3.86 eV [30, 31]. However, determining the optical band gap of MoO_3 is complicated by the presence of an additional absorption band in the range $\lambda = 330$–400 nm with a maximum at $\lambda = 350$ nm.

For nanopowder with TiO_2/V_2O_5 heterojunctions, optical absorption, judging from the measurement results, is determined by the band gap of vanadium oxide. After constructing the Kubelka–Munch function for TiO_2/V_2O_5 nanoheterostructures, it is possible to calculate that the edge of the optical absorption band is determined by a value of $E_g = 2.5 \pm 0.2$ eV, which is typical of vanadium oxide.

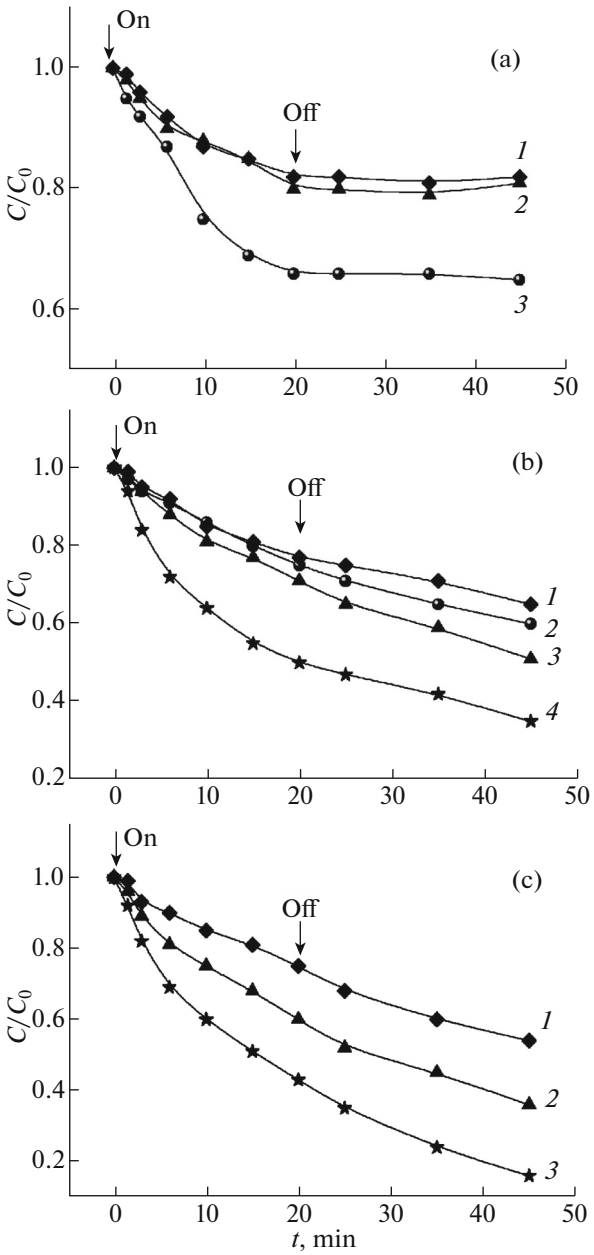

Fig. 3. Kinetics of photocatalysis for samples: (a) WO_3 (*1*), MoO_3 (*2*), TiO_2 (*3*) microspheres; (b) TiO_2/WO_3 (*1*), TiO_2/V_2O_5 (*2*), TiO_2/MoO_3 (*3*), $TiO_2/MoO_3/V_2O_5$ (*4*) microspheres; (c) TiO_2/WO_3 (*1*), TiO_2/MoO_3 (*2*), $TiO_2/MoO_3/V_2O_5$ (*3*) nanoheterostructures for photoexcitation in the visible range. Arrows show times of switching illumination on ($t = 0$) and off ($t = 20$ min). C_0, dye concentration at time $t = 0$; C, dye concentration at time t.

As noted above, the creation of multicomponent nanoheterostructures can not only affect the band gap, but also create additional radiation absorption centers and change the absorption spectra of the sam-

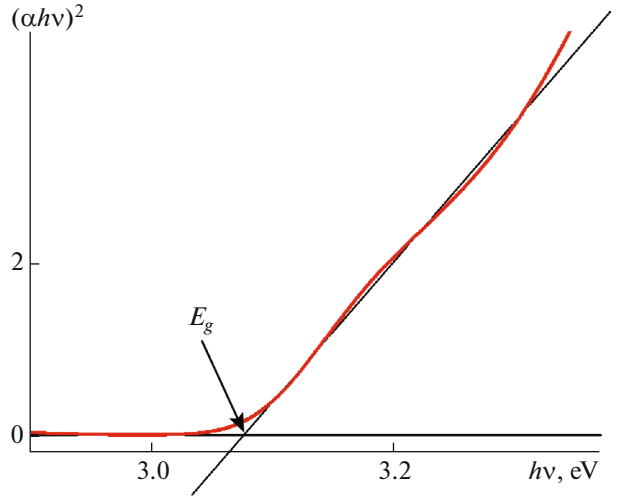

Fig. 4. (Color online) Dependence of function $(\alpha h\nu)^2$ on energy of quanta $h\nu$ and extrapolation of this dependence to determine optical band gap E_g for TiO_2 microspheres.

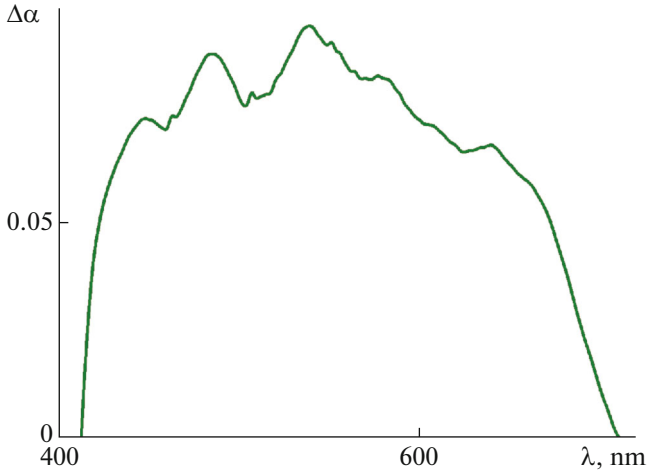

Fig. 5. (Color online) Additional absorption spectrum of TiO_2 microspheres doped with nitrogen compared with titanium dioxide not containing impurities.

ples. The difference absorption spectra of the created doped microspheres and nanoheterostructures have been studied in comparison to undoped TiO_2.

Doping of nanostructured microspheres with nitrogen atoms leads to an additional absorption line in the visible region. The corresponding difference absorption spectrum is shown in Fig. 5.

The resulting excess light absorption by TiO_2/MoO_3 nanoheterostructures in the visible region compared with pure TiO_2 nanopowder is shown in Fig. 6a; for TiO_2/V_2O_5 nanoheterostructures, in Fig. 6b. Light absorption by ternary $TiO_2/MoO_3/V_2O_5$ nanoheterostructures in the visible region is much

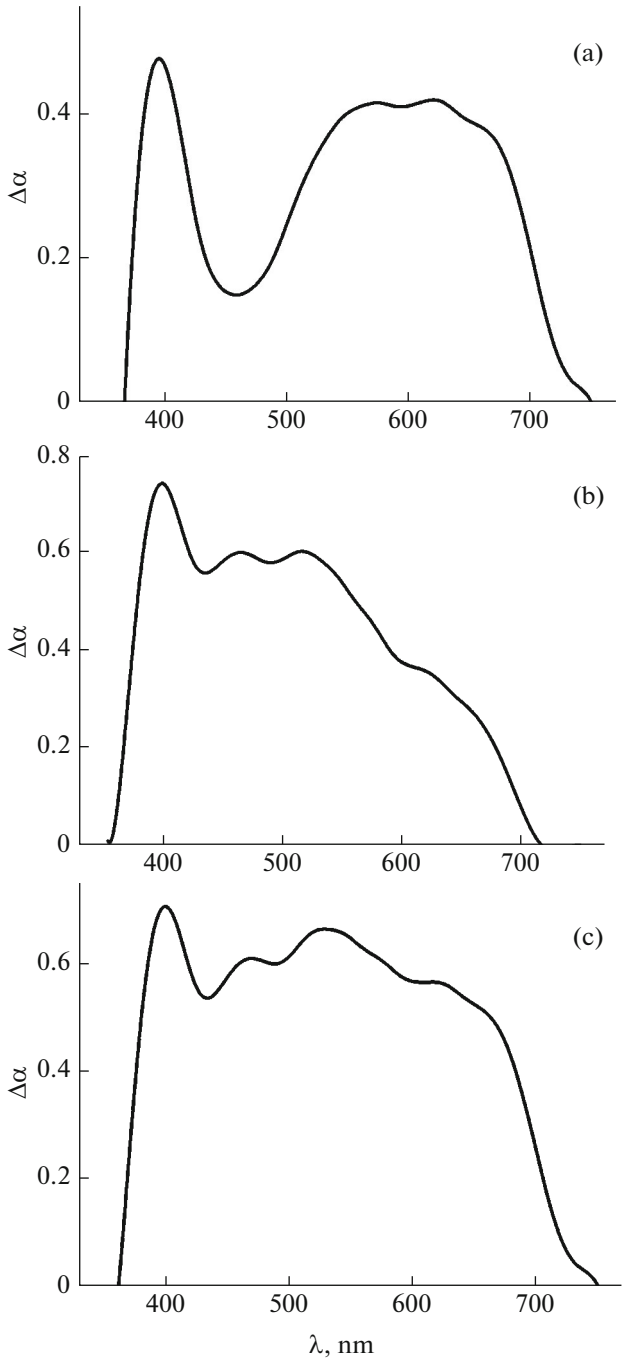

Fig. 6. Additional absorption spectrum of TiO_2/MoO_3 (a), TiO_2/V_2O_5 (b), and $TiO_2/MoO_3/V_2O_5$ (c) nanoheterostructures compared to impurity-free titanium dioxide.

higher than that of pure TiO_2. The excess light absorption by $TiO_2/MoO_3/V_2O_5$ nanopowder in the visible range compared to pure TiO_2 is shown in Fig. 6c.

Note that the concentration of radicals and the photocatalysis rate did not change during storage of all the studied samples from the time of preparation (9 months).

CONCLUSIONS

The structural, electronic, and optical properties of a series of samples of microspheres and nanoheterostructures consisting of nitrogen-doped nanocrystalline metal oxides, one of which is titanium dioxide, were obtained and investigated. It was found that all samples are characterized by a large specific surface area (about 100 m^2/g of substance) and, as a result, a high concentration of radicals, which varies over a wide range (from 10^{15} to 10^{19} g^{-1}) depending on the type of sample. It was found that the main type of radicals in the studied structures are $N^{\bullet}$, $NO^{\bullet}$, and metal ions (Ti^{3+}, Mo^{5+}, V^{4+}, W^{5+}). These defects create energy levels in the band gap of metal oxides, thereby providing an effective channel for light absorption in the visible region.

The relationship between the photocatalysis rate and concentration of radicals in a series of samples of nanostructured doped metal oxides with different morphology and chemical composition was studied for the first time. A correlation between the indicated values was revealed. The microspheres and nanoheterostructures obtained in the study, consisting of several metal oxides (one of which is titanium dioxide), have the function of accumulating photogenerated charge carriers, which is expressed in prolonged catalysis; i.e., the latter continues after illumination is turned off.

The results of this study are an important contribution to the development of new-generation energy-efficient photocatalytic devices based on nanocrystalline titanium dioxide, which operate in the visible range and do not require continuous illumination.

FUNDING

This study was financially supported by the Russian Foundation for Basic Research (project no. 18-29-23051).

CONFLICT OF INTEREST

The authors declare that they have no conflict of interest.

REFERENCES

1. B. O'Regan and M. Gratzel, Nature (London, U.K.) **335**, 737 (1991).
2. O. Oluwafunmilola and M. Maroto-Valer, J. Photochem. Photobiol., C **24**, 16 (2015).
3. T. V. Sviridova, L. Yu. Sadovskaya, E. A. Konstantinova, et al., Catal. Lett. **149**, 1147 (2019).
4. K. Sasan and F. Zuo, Nanoscale **7**, 13369 (2015).
5. X. Chen and S. Mao, Chem. Rev. **107**, 2891 (2007).
6. J. Schneider and M. Matsuoka, Chem. Rev. **114**, 9919 (2014).
7. A. Tarasov, G. Trusov, A. A. Minnekhanov, et al., J. Mater. Chem. A **2**, 3102 (2014).
8. T. V. Sviridova, L. Yu. Sadovskaya, E. M. Shchukina, et al., J. Photochem. Photobiol., A **327**, 44 (2016).
9. E. A. Konstantinova, A. A. Minnekhanov, A. I. Kokorin, et al., J. Phys. Chem. C **122**, 10248 (2018).
10. A. Tarasov, Hu. Zhi-Yi, M. Meledina, et al., J. Phys. Chem. C **121**, 4443 (2017).
11. A. Mills and S. Hunte, J. Photochem. Photobiol., A **108**, 1 (1997).
12. N. Serpone and E. Pelizzetti, *Photocatalysis: Fundamentals and Applications* (Wiley, New York, 1989).
13. M. R. Hoffmann, S. T. Martin, W. Choi, et al., Chem. Rev. **95**, 69 (1995).
14. A. Fujishima, T. N. Rao, and D. A. Tryk, J. Photochem. Photobiol., C **1**, 1 (2000).
15. A. V. Rupa, D. Divakar, and T. Sivakumar, Catal. Lett. **132**, 259 (2009).
16. R. Asahi, T. Morikawa, T. Ohwaki, et al., Science (Washington, DC, U. S.) **293**, 269 (2001).
17. Z. Barbieriková, E. Pližingrová, M. Motlochová, et al., Appl. Catal. B: Environ. **232**, 397 (2018).
18. A. A. Minnekhanov, N. T. Le, E. A. Konstantinova, et al., Appl. Magn. Reson. **48**, 335 (2017).
19. N. S. Miyamoto, R. Miyamoto, E. Giamello, et al., Res. Chem. Intermed. **44**, 4577 (2018).
20. S. Stoll and A. Schweiger, J. Magn. Reson. **178**, 42 (2006).
21. W. Wedland and H. Hecht, *Reflectance Spectroscopy* (Interscience, New York, 1966).
22. A. I. Kokorin and D. W. Bahnemann, *Chemical Physics of Nanostructured Semicontuctors* (VSP-Brill Academic, Utrecht, Boston, 2003), p. 203.
23. S. Livraghi, A. M. Czoska, M. C. Paganini, et al., J. Solid State Chem. **182**, 160 (2009).
24. A. A. Minnekhanov, D. M. Deygen, E. A. Konstantinova, et al., Nanoscale Res. Lett. **7**, 333 (2012).
25. P. C. Gravelle, F. Juillet, P. Mériaudeau, et al., Chem. Soc. Faraday Discuss. **52**, 140 (1971).
26. M. Occhiuzzi, D. Cordischi, D. Gazzoli, et al., General **269**, 169 (2004).
27. L. Lietti, I. Nova, G. Ramis, et al., J. Catal. **187**, 419 (1999).
28. R. G. Centi, E. Giamello, D. Pinelli, et al., J. Catal. **130**, 220 (1991).
29. K. I. Zamaraev, Yu. N. Molin, and K. M. Salikhov, *Spin Exchange* (Nauka, Novosibirsk, 1977) [in Russian].
30. N. V. Borisova and E. P. Surovoi, "Laws of nanosize molybdenum(VI) oxide layers optical properties change as a result of heat treatment," Bull. Tomsk. Polytech. Univ. **310** (3), 68 (2007).
31. A. L. Shkol'nik, "Optical properties of MoO_3," Izv. Akad. Nauk SSSR, Ser. Fiz. **31**, 2030 (1967).